Dong *et al. Chin. J. Mech. Eng.* (2021) 34:83
https://doi.org/10.1186/s10033-021-00601-3

Chinese Journal of Mechanical Engineering

ORIGINAL ARTICLE

Open Access

Energy-Optimal Braking Control Using a Double-Layer Scheme for Trajectory Planning and Tracking of Connected Electric Vehicles

Haoxuan Dong, Weichao Zhuang, Guodong Yin*, Liwei Xu, Yan Wang, Fa'an Wang and Yanbo Lu

Abstract

Most researches focus on the regenerative braking system design in vehicle components control and braking torque distribution, few combine the connected vehicle technologies into braking velocity planning. If the braking intention is accessed by the vehicle-to-everything communication, the electric vehicles (EVs) could plan the braking velocity for recovering more vehicle kinetic energy. Therefore, this paper presents an energy-optimal braking strategy (EOBS) to improve the energy efficiency of EVs with the consideration of shared braking intention. First, a double-layer control scheme is formulated. In the upper-layer, an energy-optimal braking problem with accessed braking intention is formulated and solved by the distance-based dynamic programming algorithm, which could derive the energy-optimal braking trajectory. In the lower-layer, the nonlinear time-varying vehicle longitudinal dynamics is transformed to the linear time-varying system, then an efficient model predictive controller is designed and solved by quadratic programming algorithm to track the original energy-optimal braking trajectory while ensuring braking comfort and safety. Several simulations are conducted by jointing MATLAB and CarSim, the results demonstrated the proposed EOBS achieves prominent regeneration energy improvement than the regular constant deceleration braking strategy. Finally, the energy-optimal braking mechanism of EVs is investigated based on the analysis of braking deceleration, battery charging power, and motor efficiency, which could be a guide to real-time control.

Keywords: Connected electric vehicles, Energy optimization, Velocity planning, Regenerative braking, Dynamic programming, Model predictive control

1 Introduction

Increasingly stringent fuel economy and emission standards in recent years promote the development of electric vehicles (EVs) [1]. However, the driving range of EVs is still too short compared with the internal combustion engine vehicle, because the battery energy density is insufficient. The short driving range is the main obstacle for the wide diffusion of EVs [2]. To extend the driving range, one of the popular ways is increasing the battery capacity, however, the battery size and vehicle price are increased simultaneously [3]. Recycling vehicle kinetic energy in the braking process is another prominent approach to extend the driving range, which is called regenerative braking in some literature [4].

Regenerative braking is the prior choice in some traffic conditions for EVs, e.g., approaching an intersection with the red signal, following the slowed preceding vehicle, and reaching a destination, because the EVs can transfer vehicle kinetic energy to electric energy by regenerative braking while without additional battery energy consumption. Since approximately 30%–50% of driving energy can be recycled in urban traffic [5], several studies have investigated regenerative braking in recent decades. Some studies tried to optimize the powertrain configuration and vehicle components for increasing regeneration energy. Hellgren et al. [6] demonstrated that

*Correspondence: ygd@seu.edu.cn
School of Mechanical Engineering, Southeast University, Nanjing 211189, China

the distributed-driven configuration of EVs has superior energy recycle potential than a central driven. Joy et al. [7] presented an integrated power circuit and electronic commutator control strategy to improve the motor generating energy of EVs. Kiddee et al. [8] designed a hybrid energy storage system, which uses the super-capacitor and lithium-ion battery to enhance the harvesting of braking energy. Zhang et al. [9] proposed an electrical-hydraulic integrated brake configuration based on the electronic stability program to achieve an efficient and safe braking system.

Another approach to improve regeneration energy is the regenerative braking strategy (RBS) design. The conventional RBS focus on braking force distribution of each wheel (axle), which cooperating with the motor braking and friction braking force to improve regeneration energy, while ensuring braking safety, stability, and comfort [10]. Sun et al. [11] integrated the braking control strategy with the objective of high braking stability and regeneration energy, which including three braking force operating modes. Xu et al. [12] presented two regenerative braking force optimization controllers to promote regeneration energy, it considering motor efficiency to distribute the friction and motor braking torque of the front and rear wheels. Li et al. [13] proposed a composite RBS to optimize regenerative and plugging braking simultaneously with the driver's intention recognition. Lian et al. [14] designed an optimal braking force distribution strategy, while uses a safety distance model to avoid collision. In addition, the rule-based algorithm [9], PID algorithm [15], sliding mode control [16], fuzzy logic control [17], design of experiment method [11], model predictive control (MPC) [12], and dynamic programming (DP) algorithm [18] were adopted to refine the RBS.

Recently, the emerging of connected vehicle technologies, i.e., vehicle-to-everything (V2X) communication, provides possibilities to further improve energy efficiency and reduce emission [19]. The traffic, road, and vehicle information can be accessed by V2X, which is used to plan the energy-optimal velocity, i.e., the surrounding vehicle states [20], road slope [21], road curvature [22], and traffic signal phase and timing [23]. However, most researches focus on the RBS design in vehicle components control and braking torque distribution, few combine the connected vehicle technologies into braking velocity planning. If the braking intention is accessed by the V2X (i.e., braking distance and terminal velocity), the EVs could plan the braking velocity for recovering more energy.

Therefore, this paper proposes an energy-optimal braking strategy (EOBS), where the key is using shared braking intention to planning energy-optimal braking trajectory. The major contributions of this paper are threefold. First, a double layer control scheme is proposed: in the upper-layer, the energy-optimal braking trajectory is planned by the distance-based DP for fast computation. Second, to follow the optimal trajectory, the lower-layer designs a tracking controller using the linear time-varying MPC (LTV-MPC), to minimize the trajectory tracking errors while ensuring braking comfort and safety. Third, the mechanism of energy-optimal braking is derived. The energy-optimal braking trajectory is consists of multiple phases, which can be converted to a rule-based braking strategy.

The remainder of this paper is organized as follows. Section 2 introduces the EVs model and regenerative braking strategy. Section 3 formulates the energy-optimal braking problem and double-layer EOBS. Section 4 verifies the performance of the proposed EOBS, and investigates the energy-optimal braking mechanism. Finally, conclusions are presented in Section 5.

2 Vehicle Model and Regenerative Braking Strategy

2.1 Vehicle Model

This paper optimizes the braking velocity of four-wheel-independent-driven electric vehicles, which is powered by four in-wheel motors (IWM).

2.1.1 Vehicle Dynamics

This paper focuses on the energy-optimal braking control problem in the context of daily driving on a straight and high adhesion road. Therefore, only the longitudinal dynamics is modeled, as shown in Eq. (1):

$$\dot{x} = f(x,\ u) = \begin{bmatrix} 0 & 1 \\ 0 & -\frac{0.5C_D A_r \rho v^2 + mgf\cos\theta + mg\sin\theta}{\delta m v} \end{bmatrix} x + \begin{bmatrix} 0 \\ \frac{1}{\delta m} \end{bmatrix} u, \quad (1)$$

where m is the vehicle mass, δ is the vehicle rotational inertia coefficient, g is the acceleration of gravity, θ is the road slope, f is the rolling resistance coefficient, C_D is the aerodynamic drag coefficient, A_r is the frontal area, and ρ is the air density. $x = [d\ v]^{\mathrm{T}}$ is the states variable, d is the distance, v is the velocity. $u = F$ is the control variable, F is the vehicle force, positive for traction force and negative for braking force.

In the traction process, the vehicle force is supplied by IWM, i.e., $F = \sum F_m$. In the braking process, the vehicle force including motor force F_m and friction braking force F_f, i.e., $F = \sum F_m + \sum F_f$. In this paper, the dynamics of the motor is not mainly considered, so the motor response model is simplified by using first-order lag relation

$$\tau_m \dot{F}_m + F_m = F_{md}, \quad (2)$$

where F_{md} is the desired motor force, which is derived by regenerative braking strategy. τ_m is the motor time constant coefficient.

The friction braking force is generated by a hydraulic brake system (HBS). We also use the first-order lag relation to represent the HBS response, i.e.,

$$\tau_h \dot{p}_w + p_w = p_{wd}, \tag{3}$$

where p_w is the brake wheel cylinder pressure, τ_h is the HBS time constant coefficient. p_{wd} is the desired brake wheel cylinder pressure, which is calculated by Eq. (4):

$$p_{wd} = F_f r_w \kappa, \tag{4}$$

where κ is the conversion coefficient of wheel cylinder pressure, r_w is the radius of the wheel.

2.1.2 Energy Consumption

The power of motor is calculated by Eq. (5)

$$P_m = \frac{F_m r_w n}{9.55}, \tag{5}$$

where P_m is the instantaneous motor power, positive for propulsion power and negative for generation power. n is the motor rotational speed.

This paper ignores the energy losses in electric wires and considers the accessory power P_a. Then the battery power P_b is

$$P_b = \sum P_m \eta_m^{-\mathrm{sign}(P_m)} \eta_b^{-\mathrm{sign}(P_m)} + P_a \eta_b^{-1}, \tag{6}$$

where P_a is the power consumption by the vehicle accessories, e.g., vehicle headlight, air conditioning, assisted motor of the steering system, etc. η_b is the battery efficiency, sign(·) is the signum function, η_m is the motor efficiency which is determined by the motor torque and speed as shown in Figure 1.

The battery is modeled as a simple equivalent circuit [24], which charging current I_b is expressed as Eq. (7)

$$I_b = \frac{E - \sqrt{E^2 - 4R_o P_b}}{2R_o}, \tag{7}$$

where E is the open-circuit voltage, and R_o is the internal resistance. The battery state of charge (SOC) can be calculated by Eq. (8)

$$SOC = SOC_0 + \frac{\int I_b \mathrm{d}t}{3600 C_b}, \tag{8}$$

where SOC_0 is the battery initial SOC, C_b is the battery capacity.

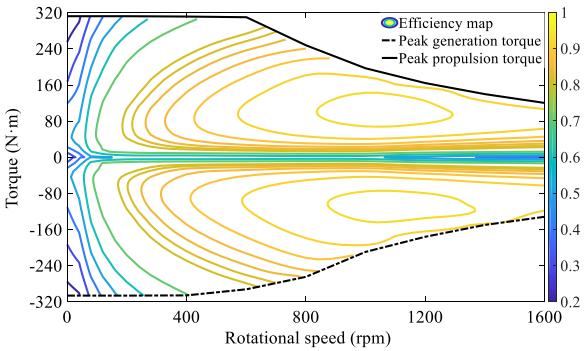

Figure 1 The efficiency map and peak torque of IWM

2.2 Regenerative Braking Strategy

The RBS including twofold: braking force distribution on the front and rear axles, motor and friction braking force distribution on each wheel. The distributed braking force on the front and rear axles affect braking stability, then we use 'ideal distribution strategy' to prevent wheel locking [25]

$$F_{bf} = \beta F, \tag{9}$$

$$F_{br} = (1 - \beta) F, \tag{10}$$

where F_{bf} and F_{br} are the braking force on the front and rear axle, respectively. β is the ideal distribution ratio, which is proportional to vehicle axle normal forces

$$\beta = \frac{(L_b + z h_g)}{L_w}, \tag{11}$$

where L_b is the distance from the rear axle to the center of vehicle mass, L_w is the vehicle wheelbase, h_g is the distance from the ground to the center of vehicle mass, z is the brake strength.

We assume the vehicle driving on the straight road, then the braking force on the left and right wheels are identical. The motor force is preferred to recycle more energy, and HBS provides the remained force while the motor force can not meet the demand. For an example of the front-rear wheel, the motor and friction braking force are calculated by Eqs. (12) and (13), respectively:

$$F_{md} = \min\left(F_{m\max},\ 0.5 F_{bf}\right), \tag{12}$$

$$F_f = 0.5 F_{bf} - F_m, \tag{13}$$

where $F_{m\max}$ is motor maximum braking force.

3 Energy-optimal Braking Strategy

This section formulates the energy-optimal braking problem and proposes a double-layer EOBS to improve regeneration energy while ensuring braking comfort and safety. In the upper-layer, the energy-optimal braking trajectory is planned by solving the optimal control problem. In the lower-layer, a tracking controller is used to track the optimized trajectory accurately while ensuring braking comfort and safety. Figure 2 shows the scheme of the proposed double-layer EOBS.

3.1 Energy-optimal Braking Trajectory Planning

The energy-optimal braking trajectory is planned by the DP algorithm. Since the DP has been widely used in the energy optimization problem [19], which divides the optimal control problem into simpler sub-problems and calculates recursively based on the Bellman optimality principle [26].

3.1.1 Optimization Problem Formulation

Figure 3 shows the scenario of braking, where D is the distance to the destination (can be a stop line of the signalized intersection or a stopped preceding vehicle), V_s and V_e are the initial and desired terminal velocity, respectively. We assume the D and V_e are accessed by V2X communication, the V_s is obtained by using on-board sensors.

In this paper, the braking distance D is fixed, thus the whole problem is discretized in distance-domain by distance step Δd. The total number of distance step N_D is determined by the D and Δd, i.e., $N_D = D/\Delta d + 1$. The velocity is selected as the state variable, i.e., $x_D = v$, and the braking deceleration a is selected as the control variable, i.e., $u_D = a$. Since the distance step is small, the braking deceleration of each sub-problem is assumed to be constant. Thus, the energy-optimal braking problem is expressed in Eq. (14) indexed by k:

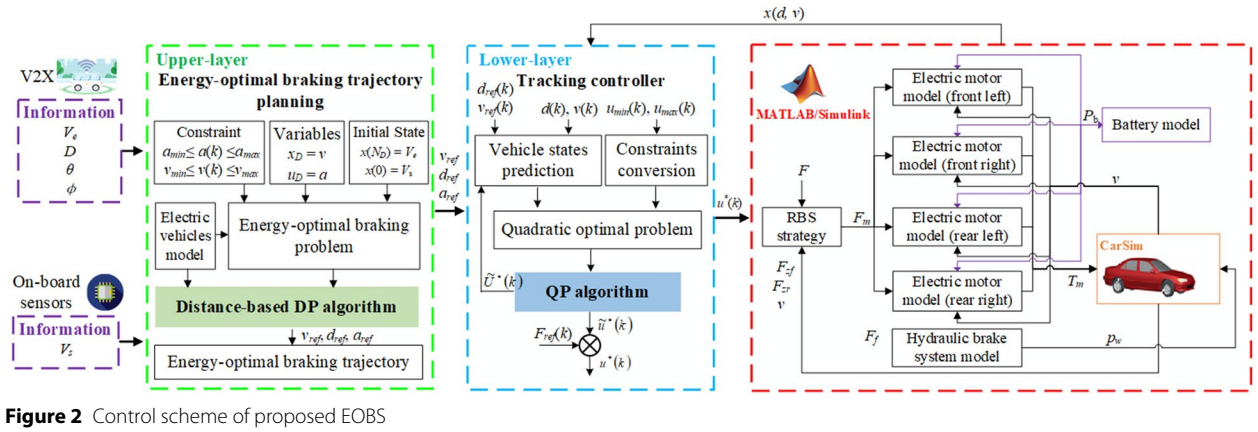

Figure 2 Control scheme of proposed EOBS

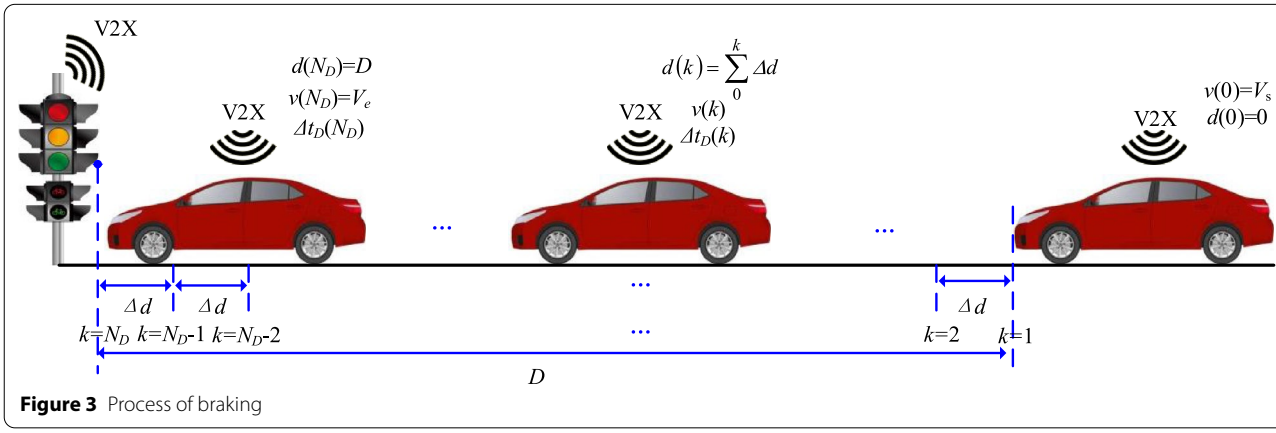

Figure 3 Process of braking

$$\begin{aligned}&\underset{u_D\in U}{\text{Minimum}}\ J_D(x_D(k),u_D(k))\\&=\sum_{k=1}^{k=N_D}P_b(k)\Delta t_D(k)+\alpha(v(N_D)-V_e)^2,\end{aligned}\tag{14}$$

s.t.,
$x_D(0)=V_s$,
$x_D(N_D)=V_e$,
$v(k)\in[v_{\min},v_{\max}]$,
$u_D(k)\in[a_{\min},a_{\max}]$, where $v_{\min}$ and $v_{\max}$ are the minimum velocity for efficient traffic and the maximum velocity for road limitation, respectively. $a_{\min}$ and $a_{\max}$ are the deceleration depend on braking comfort and vehicle resistance, respectively. Δt_D is the time interval. Note that the terminal condition of the velocity has been relaxed by converting them to soft constraints and merged into the objective function as Eq. (14), with weighting factor α for the latter term.

Besides, the state transfer of vehicle velocity and time interval in k step are calculated by Eqs. (15) and (16), respectively.

$$v(k+1)=\begin{cases}\sqrt{v^2(k)+2a(k)\Delta d}, & v^2(k)+2a(k)\Delta d>0,\\ 0, & v^2(k)+2a(k)\Delta d\le 0,\end{cases}\tag{15}$$

$$\Delta t_D(k)=\frac{v(k+1)-v(k)}{a(k)}.\tag{16}$$

3.1.2 DP Solving

Denote the transitional cost-to-go function from k step to k+1 step $W(x_D(k), u_D(k))$ and the penalty function for the terminal states $G(x_D(N_D))$, i.e.,

$$W(x_D(k),u_D(k))=P_b(k)\Delta t_D(k),\tag{17}$$

$$G(x_D(N_D))=\alpha(v(N_D)-V_e)^2.\tag{18}$$

The formulated control problem is solved recursively by following the Bellman optimality principle [[26]]:
N_D-1 step:

$$J^*_{N_D-1}(x_D(N_D-1))\tag{19}$$

$$\min_{u_D\in U}\{W(x_D(N_D-1),u_D(N_D-1))+G(x_D(N_D))\},$$

k step:

$$J^*_k(x_D(k))=\min_{u_D\in U}\left\{W(x_D(k),u_D(k))+J^*_{k+1}(x_D(k+1))\right\},\tag{20}$$

where $J^*_k(x_D(k))$ is the minimum cost-to-go value at the moment k. Then, the energy-optimal braking trajectory and control law can be obtained by backward calculation.

3.2 Tracking Controller

3.2.1 Tracking Problem Formulation

The objective of the tracking controller is to minimize the tracking error between the actual and original optimal trajectory, while adapts to traffic conditions for braking comfort and safety. In this paper, the vehicle velocity and distance error and vehicle force increment are defined as soft constraints, thus, the tracking problem is shown in Eq. (21):

$$\begin{aligned}\underset{u_M\in U}{\text{Minimum}}\ J_M(u_M|k)=&\sum_{i=1}^{N_p}\left\|\tilde{x}(k+i|k)\right\|_Q^2\\&+\sum_{j=1}^{N_c-1}\left\|\Delta u(k+j|k)\right\|_R^2+\beta\varepsilon^2,\end{aligned}\tag{21}$$

s.t.,
$u_{\min}(k+j)\le u_M(k+j)$,
$D-L\le d(N_M)\le D$,
$V_e-\vartheta\le v(N_M)\le V_e$,
where $\tilde{x}=[d-d_{ref},\ v-v_{ref}]$ is the vehicle states error. d_{ref} and v_{ref} are the original distance and velocity in the upper-layer solution, respectively, which are derived from the upper-layer optimization. Δu is the increment of the control variable, $(u_M|k)$ represents the derived control variable of the controller at k moment. Q, R, and β are the weighing factor matrix, ε is the relaxation factor, N_p and N_c are the prediction horizon and control horizon, respectively. N_M is the tracking problem horizon, which is determined by the length of the original trajectory. L is the vehicle length, ϑ is the velocity slack.

In tracking problem Eq. (21), the constraints including twofold. First, the vehicle force is subject to physical limits $u_{\min}$, which is determined by the maximum comfort braking force and road adhesion. Secondly, the virtual stop region that including distance and velocity is defined as a buffer space that relies on safety distance and minimum steady velocity of EVs, then the actual terminal braking distance and velocity are meet the second and third constraints.

3.2.2 Linear Time-varying State Prediction Model

Since the vehicle dynamics in Eq. (1) is nonlinear, it greatly increases the computational burden of MPC. Therefore, we employ the approximate linearization method [27] to transform the nonlinear time-varying model Eq. (1) to a linear time-varying (LTV) system:

$$\dot{\tilde{x}} = \begin{bmatrix} 0 & 1 \\ 0 & -\frac{C_D A_r \rho v_{ref}}{\delta m} \end{bmatrix} \tilde{x} + \begin{bmatrix} 0 \\ \frac{1}{\delta m} \end{bmatrix} \tilde{u} \tag{22}$$

where $\tilde{x} = \begin{bmatrix} d - d_{ref} & v - v_{ref} \end{bmatrix}^{\mathrm{T}}$, $\tilde{u} = \begin{bmatrix} F - F_{ref} \end{bmatrix}^{\mathrm{T}}$, F_{ref} is the original braking force, which calculated by Eq. (23):

$$F_{ref} = mgf\cos\theta + mg\sin\theta + 0.5 C_D A_r \rho v_{ref}^2(k) + m\delta a_{ref}(k). \tag{23}$$

Since the MPC calculates the control law discretely, the LTV system in Eq. (22) is converted to the discrete-time system using the Euler method [28]:

$$\tilde{x}(k+1) = \begin{bmatrix} 1 & \Delta t_M \\ 0 & 1 - \frac{C_D A_r \rho v_{ref}(k) \Delta t_M}{\delta m} \end{bmatrix} \tilde{x}(k) + \begin{bmatrix} 0 \\ \frac{\Delta t_M}{\delta m} \end{bmatrix} \tilde{u}(k), \tag{24}$$

where Δt_M is the time step.

Denote a state prediction matrix:

$$\varsigma(i+1|k) = \begin{bmatrix} \tilde{x}(i|k) \\ \tilde{u}(i-1|k) \end{bmatrix}, \tag{25}$$

where $(i|k)$ represents the i-step-ahead predicted error at the kth step. Substituting Eq. (24) into Eq. (25), a new state-space model is derived:

$$\begin{cases} \varsigma(i+1|k) = A_{k,i}\varsigma(i|k) + B_{k,i}\Delta\tilde{u}(i|k), \\ \upsilon(i|k) = C_{k,i}\varsigma(i|k), \end{cases} \tag{26}$$

with

$$A_{k,i} = \begin{bmatrix} 1 & \Delta t_M & 0 \\ 0 & 1 - \frac{C_D A_r \rho v_{ref}(i|k) \Delta t_M}{\delta m} & \frac{\Delta t_M}{\delta m} \\ 0 & 0 & 1 \end{bmatrix},$$

$$B_{k,i} = \begin{bmatrix} 0 & \frac{\Delta t_M}{\delta m} & 1 \end{bmatrix}^{\mathrm{T}},$$

$$C_{k,i} = \begin{bmatrix} 1 & 0 & 0 \\ 0 & 1 & 0 \end{bmatrix}.$$

Finally, the state prediction model is listed in Eq. (27) by converting Eq. (26):

$$\tilde{Y}(k) = \Gamma_k \varsigma(k) + \Xi_k \Delta\tilde{U}(k), \tag{27}$$

with

$$\tilde{Y}(k) = \begin{bmatrix} \upsilon(k+1|k) & \cdots & \upsilon(k+N_c|k) & \cdots & \upsilon(k+N_p|k) \end{bmatrix}^{\mathrm{T}}_{1\times N_p},$$

$$\Delta\tilde{U}(k) = \begin{bmatrix} \Delta\tilde{u}(k|k) & \Delta\tilde{u}(k+1|k) & \cdots & \Delta\tilde{u}(k+N_c|k) \end{bmatrix}^{\mathrm{T}}_{1\times N_c},$$

$$\Gamma_k = \begin{bmatrix} C_{k,i}A_{k,i} & \cdots & C_{k,i}A_{k,i}^{N_c} & \cdots & C_{k,i}A_{k,i}^{N_p} \end{bmatrix}_{1\times N_p},$$

$$\Xi_k = \begin{bmatrix} C_{k,i}B_{k,i} & 0 & \cdots & 0 \\ C_{k,i}A_{k,i}B_{k,i} & C_{k,i}B_{k,i} & \cdots & 0 \\ \vdots & \vdots & \ddots & \vdots \\ C_{k,i}A_{k,i}^{N_c}B_{k,i} & C_{k,i}A_{k,i}^{N_c-1}B_{k,i} & \cdots & C_{k,i}A_{k,i}B_{k,i} \\ \vdots & \vdots & \ddots & \vdots \\ C_{k,i}A_{k,i}^{N_p-1}B_{k,i} & C_{k,i}A_{k,i}^{N_p-2}B_{k,i} & \cdots & C_{k,i}A_{k,i}^{N_p-N_c-1}B_{k,i} \end{bmatrix}_{N_p\times N_c},$$

where $\tilde{Y}(k)$ and $\Delta\tilde{U}(k)$ are output and control increments of the prediction model, respectively. Noted that according to the principle of MPC, the $N_c \le N_p$, and the control input that beyond N_c is equal to the last control input of N_c.

3.2.3 Quadratic Programming Solving

The tracking problem is solved using the quadratic programming (QP) algorithm. Then, the objective function and constraints in Eq. (21) are converted to standard QP form Ref. [29], i.e.,

$$\begin{aligned} J_M\left(\Delta\tilde{U}|k\right) = & \frac{1}{2}\begin{bmatrix} \Delta\tilde{U}(k)^{\mathrm{T}} \\ \varepsilon \end{bmatrix}\begin{bmatrix} 2\left(\Xi_k^{\mathrm{T}} Q \Xi_k + R\right) & 0 \\ 0 & 2\beta \end{bmatrix} \\ & \begin{bmatrix} \Delta\tilde{U}(k)^{\mathrm{T}} \\ \varepsilon \end{bmatrix}^{\mathrm{T}} \\ & + \begin{bmatrix} 2E_k^{\mathrm{T}} Q \Xi_k \\ 0 \end{bmatrix}^{\mathrm{T}}\begin{bmatrix} \Delta\tilde{U}(k)^{\mathrm{T}} \\ \varepsilon \end{bmatrix}^{\mathrm{T}} \end{aligned} \tag{28}$$

s.t.,

$$D - L \le d(N_M) \le D,$$

$$V_e - \vartheta \le v(N_M) \le V_e,$$

$$U_{\min} \le \begin{bmatrix} 1 & \cdots & 0 \\ \vdots & \ddots & \vdots \\ 1 & \cdots & 1 \end{bmatrix}_{N_c\times N_c} \Delta\tilde{U}(k) + 1_{Nc}\Delta\tilde{u}(k-1),$$

where 1_{Nc} is the column vector with N_c rows, $U_{\min}$ is the minimum value set of control input

$$U_{\min} = \begin{bmatrix} u_{\min}(k) & u_{\min}(k+1) & \cdots & u_{\min}(k+N_c-1) \end{bmatrix}^{\mathrm{T}}_{1\times N_c}. \tag{29}$$

A series of control input increments $\Delta\tilde{U}_k^*$ in the control horizon can be obtained by solving the QP problem. The predicted control input $\tilde{u}^*(k)$ is the first term of the control sequence plus the previous control input $\tilde{u}(k-1)$:

$$\tilde{u}^*(k) = \tilde{u}(k-1) + \begin{bmatrix} I_{N_c} & 0 & \cdots & 0 \end{bmatrix}_{1\times N_c}\Delta\tilde{U}_k^*. \tag{30}$$

Finally, the predicted vehicle braking force $u^*(k)$ is

$$u^*(k) = \tilde{u}^*(k) + F_{ref}(k). \tag{31}$$

4 Simulation Results and Discussion

In this section, a simulation is conducted by jointing MATLAB (version 9.4, R2018a) and CarSim (version 20959, 2016.1) on a PC with an Intel Core i7-8700 @ 3.20 GHz CPU, the joint simulation structure as shown in Figure 2. In addition, the index α_r is defined to evaluate the performance of regeneration efficiency as described in Eq. (32) [9]:

$$\alpha_r = \frac{\int P_b \mathrm{d}t}{0.5m\delta\left(V_s^2 - v_e^2\right)} \times 100 \tag{32}$$

where v_e is the actual terminal velocity in the lower-layer.

4.1 Simulation Setup

The EVs model is established using C-Class hatchback 2012 vehicle in CarSim, and the main parameters of EVs are $f=0.016$, $m=1421$ kg, $C_D=0.3$, $A_r=2.22$ m^2, $r_w=0.325$ m, $\rho=1.206$ kg/m^3, $g=9.8$ m/s^2, $\delta=1.022$, $L=4.85$ m, $L_w=2.91$ m, $L_b=1.9$ m, $h_g=0.54$ m, and $P_a=300$ W. The specifications of IWM are the peak propulsion power and generation power are 20.75 kW and -20.53 kW, respectively. The peak propulsion torque and generation torque are 312.50 N·m and -311.50 N·m, respectively, and the peak rotational speed is 1600 r/min. The specifications of battery are $E=360$ V, $C_b=140$ A·h, $R_o=0.45$ Ω, $SOC_0=0.8$, and $\eta_b=0.9$. According to the HBS module in CarSim, the τ_h of all wheels is 0.06, the κ of wheels in front axle and rear axle are 250 MPa/(N·m) and 150 MPa/(N·m), respectively.

In the DP optimization, the distance step $\Delta d=0.01$ m, the grid step of state variable v and control variable a are 0.1 m/s and 0.05 m/s^2, respectively. In the LTV-MPC controller, the lengths of prediction horizon N_p and control horizon N_c both are 100, which finds a good compromise between optimality and computational efficiency, as verified by a systematic simulative analysis for various horizon lengths. The weight matrices are $Q=1000I_{2Np\times 2Np}$ and $R=200I_{Nc}$, and the sampling time $\Delta t_M=0.01$ s.

Two typical braking scenarios are simulated to evaluate the regeneration energy efficiency of the proposed strategy. The scenarios are referred to as Scenarios A and B, i.e., normal braking with small deceleration and emergency braking with big deceleration. The main parameters of these two scenarios are listed in Table 1.

Table 1 Braking scenarios

	Scenario A	Scenario B
Initial velocity V_s (m/s)	34	20
Terminal velocity V_e (m/s)	20	0
Distance to destination D (m)	204	50
Adhesion coefficient φ	0.85	
Velocity slack ω (m/s)	0.2	
Safety distance slack ϑ (m)	4.85	
Road adhesion θ	0	

4.2 Benchmark Strategy

The proposed EOBS is compared with the regular constant deceleration braking strategy (CDBS) for benchmarking proposes. For CDBS [30], the vehicle will brake by using a constant deceleration, and the lower-layer uses the same LTV-MPC controller as the proposed EOBS to track the constant deceleration velocity trajectory. The trajectory tracking performance in the sense of regeneration energy optimality and braking safety is evaluated by comparing the LTV-MPC controller with the PID controller. For the PID controller, the velocity error is used as the input and the deceleration is defined as the output to achieve speed tracking. In addition, we define the original solution of the upper-layer as the original trajectory. While the safety-guaranteed solution in the lower-layer is defined as the actual trajectory.

4.3 Performance of the Proposed EOBS

4.3.1 Tracking Performance

The tracking performance of the LTV-MPC controller will be verified in Scenario A, and compared with the regular PID controller. The LTV-MPC and PID controller is used to track the same original trajectory derived in the upper-layer of EOBS. Figures 4, 5, 6 and Table 2 are the simulation results.

Figure 4 shows the vehicle trajectory of distance and velocity, Figures 5 and 6 show the vehicle braking force and slip rate, respectively. The regeneration energy, vehicle terminal states are listed in Table 2. In Figure 4 and Table 2, the actual terminal velocity and braking distance error of the LTV-MPC controller are 0.01 m/s and 0.03 m respectively, and 0.72 m/s and 9.96 m of PID controller. The error data shows better tracking performance of the LTV-MPC controller than the PID controller. The distance exceeds the maximum permissible distance (201.58–196.73 m) in the PID controller, which causes collision possibly. Figure 5 shows the braking force both do not exceed constraints of LTV-MPC and PID controller, however, the PID controller leads to a large tracking error, which is the cause of state tracking error as shown in Figure 4. Figure 6 shows the small slip rate of each wheel, which indicates the braking stability is still ensured by employing the LTV-MPC.

As shown in Table 2, the vehicle with the LTV-MPC controller achieves regeneration energy efficiency increase by 3.83% compared with the PID controller,

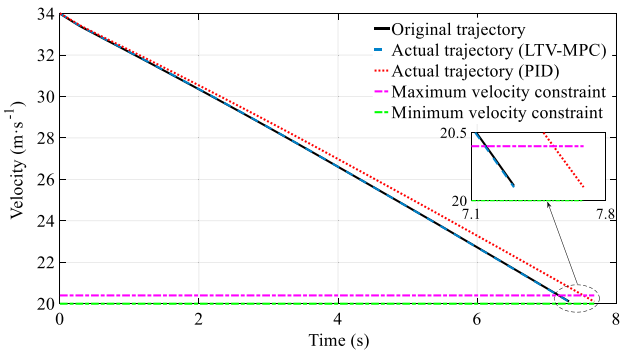

(a) Velocity trajectory

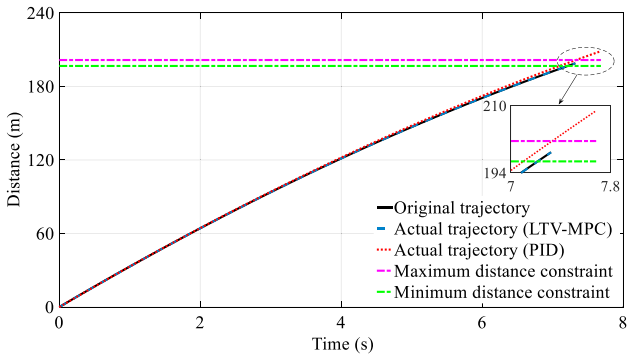

(b) Distance trajectory

Figure 4 Braking trajectory of EVs

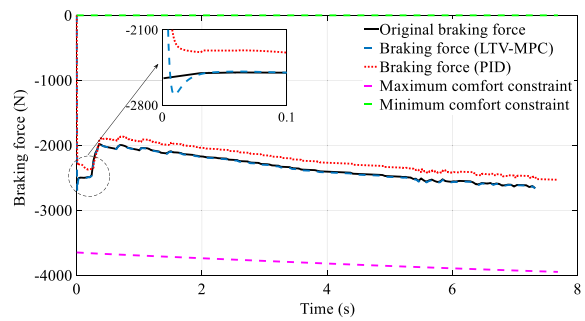

Figure 5 Braking force of EVs

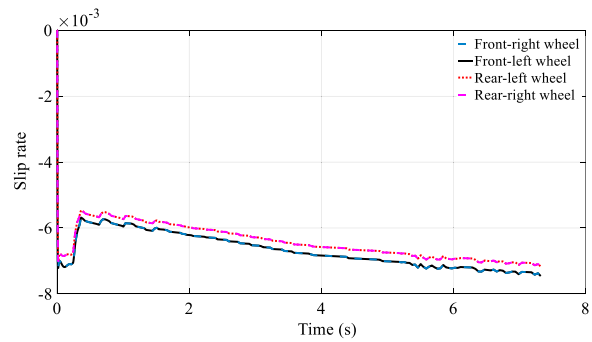

Figure 6 Slip rate of EVs by LTV-MPC

and decreases by 0.03% compared with the original trajectory. Thus, the regeneration energy efficiency of the LTV-MPC controller is superior to the PID controller, because of the excellent tracking performance.

4.3.2 Regeneration Energy Efficiency

The regeneration energy efficiency of EOBS is evaluated by compared with CDBS in Scenarios A and B. The simulation results are shown in Figure 7 and Table 3. Figure 7 shows the braking deceleration. The braking deceleration of CDBS is constant (e.g., Scenario A is -1.89 m/s^2 and Scenario B is -4.26 m/s^2, which is the average deceleration of EOBS), while the EOBS derives a varied deceleration for energy-optimal consideration. Table 3 shows the regeneration energy and vehicle terminal states of EOBS and CDBS. We can observe the vehicle could stay within the defined region in Scenarios A and B, and the proposed EOBS has improved the regeneration energy in Scenario A and Scenario B by 11.42% and 3.19% than CDBS.

These above-mentioned results show that the proposed EOBS guarantees braking safety, while improving regeneration energy, especially in normal braking scenario. Further, the energy-optimal braking mechanism of EVs will be analyzed in detail in Section 4.4.

Table 2 Simulation result of LTV-MPC and PID controller

	Regeneration energy efficiency α_r (%)	Braking duration (s)	Distance d (m)	Terminal velocity v_e (m/s)
Original trajectory	68.21	7.30	198.85	20.09
LTV-MPC controller	68.18	7.32	198.88	20.10
PID controller	64.35	7.68	208.81	20.13

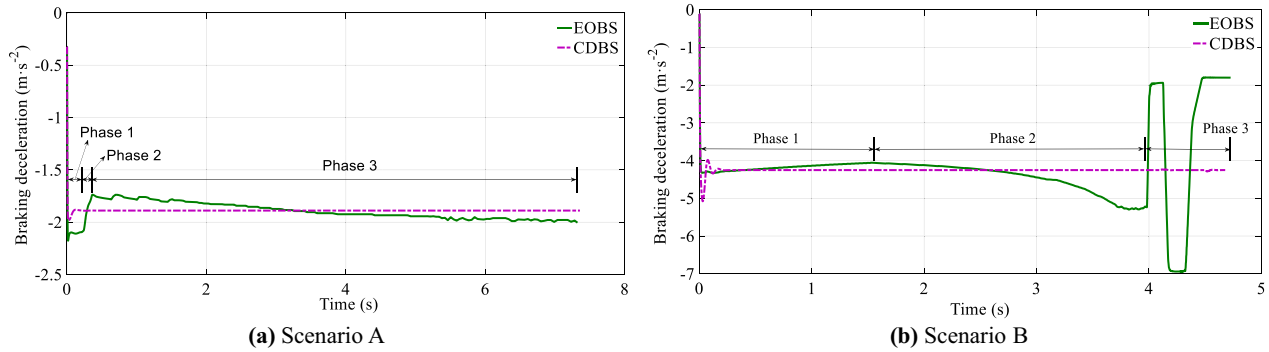

Figure 7 Simulation results of braking deceleration

Table 3 Simulation results of EOBS and CDBS

		Regeneration energy efficiency α_r (%)	Improvement (%)	Distance d (m)	Terminal velocity v_e (m/s)
Scenario A	EOBS	68.18	11.42	198.88	20.10
	CDBS	56.76	N/A	198.94	20.10
Scenario B	EOBS	44.61	3.19	46.97	0.10
	CDBS	41.42	N/A	47.13	0.11

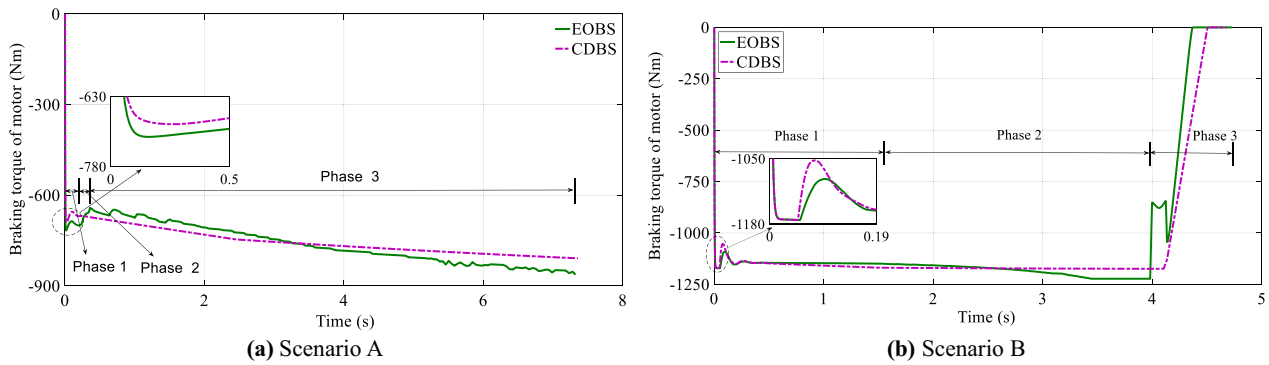

Figure 8 Braking torque of motor

4.4 Energy-optimal Braking Mechanism

Figures 8, 9, 10 are the motor braking force, braking cylinder pressure of HBS (the sum of every wheel), and battery charging power, respectively. The motor efficiency during the regenerative braking and its average value are listed in Table 4.

In Scenario A, as shown in Figure 7a, the deceleration of EOBS including three phases: increasing firstly, then decreasing, and increasing again. The wheel cylinder pressure increases firstly and then drops to approximately zero in the second and third phases (see Figure 9a). In the first phase, a large braking deceleration is operated. Although the friction braking force increased with the large deceleration (see Figure 9a), the battery charging power is increased. This means that the vehicle can make full use of the peak generation power to recover more vehicle kinetic energy. The second and last phases of EOBS should be discussed together because these two phases are complementary compared to CDBS. Figures 8a and 10a illustrate

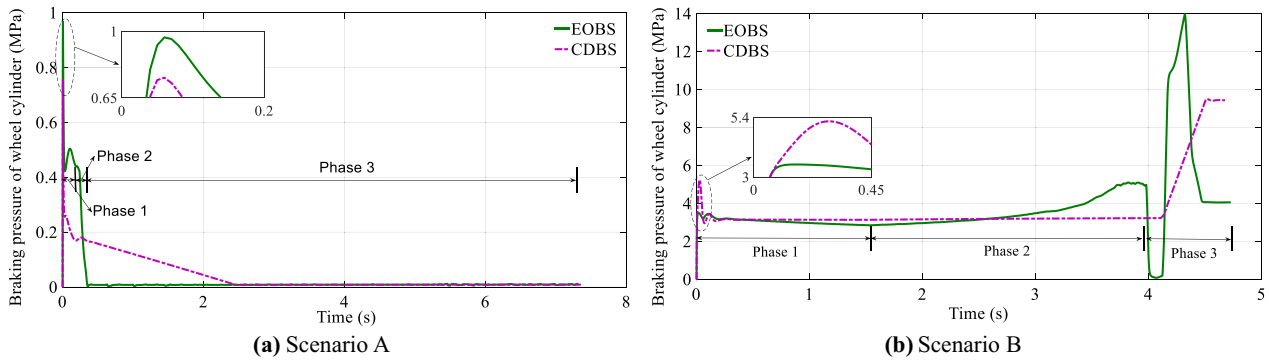

(a) Scenario A **(b)** Scenario B

Figure 9 Wheel cylinder pressure of HBS

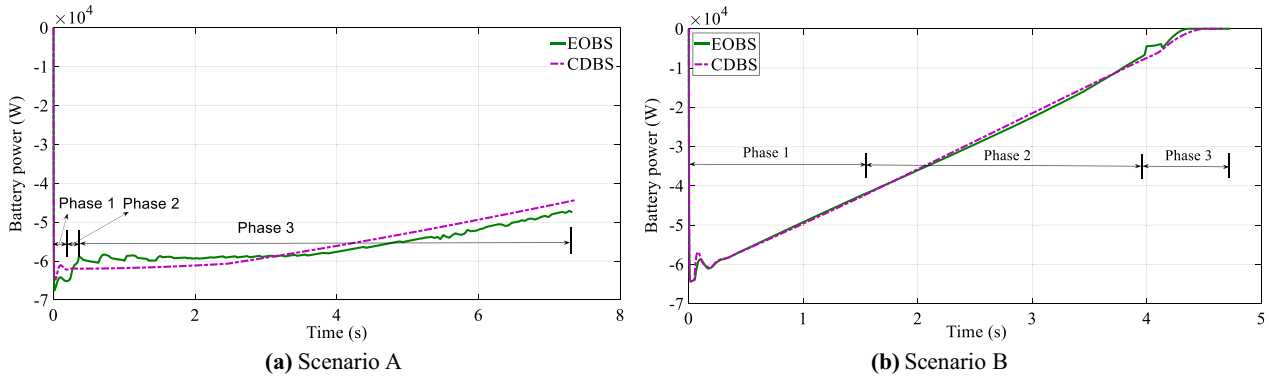

(a) Scenario A **(b)** Scenario B

Figure 10 Battery charging power

Table 4 Efficiency of motor (%)

		Front axle Left/right wheel	Rear axle Left/right wheel	Average efficiency
Scenario A	EOBS	90.59	87.73	89.16
	CDBS	90.55	87.75	89.15
Scenario B	EOBS	77.99	77.93	77.96
	CDBS	79.49	79.49	79.49

a complementary relationship: the motor braking force, battery charging power of EOBS less than CDBS in the second phase, but larger than CDBS in the last phase. In the second phase, the braking deceleration decreases quickly to reduce friction braking force (see Figure 9a). In the last phase, to make full use of the motor (see Figures 8a, 10a), the braking deceleration of EOBS increases.

In Scenario B, as shown in Figure 7b, the braking deceleration of EOBS can be divided into three phases same as Scenario A and for the same reasons. The first and second phases are discussed together, in the first phase, the deceleration of EOBS decreases and increases in the second phase. In the third phase, the braking deceleration decreases because the motor generating force is gradually dwindling and replaced by the friction braking force in low-speed operating conditions (see Figures 8b and 9b). As shown in Figure 10b, the battery charging power of EOBS and CDBS are similar, which causes the regeneration energy improvement of EOBS is not obvious in the emergency braking case (see Table 3).

In addition, Table 4 shows the motor efficiency of EOBS and CDBS. The average motor efficiency in EOBS is greater than CDBS in Scenario A, but it less than CDBS in Scenario B. This phenomenon indicates only focus on maximum motor working efficiency does not mean maximum regeneration energy. The regeneration energy is related to motor generation power and motor efficiency, and the co-optimization of motor generating power and motor efficiency is the key to achieve the energy-optimal braking control. Therefore, the energy-optimal braking control requires reasonably reducing friction braking force and increasing motor braking force for improving

the motor generation power, and operating the motor working at a high-efficiency point at the same time.

5 Conclusions

This paper presented a double-layer energy-optimal braking strategy to improve the regeneration energy using accessed braking intention. First, the energy-optimal braking trajectory is derived by distance-based dynamic programming in the upper-layer. Then, in the lower-layer, the linear time-varying model predictive controller is formulated to follow the optimal trajectory accurately while ensures braking safety and comfort. The simulation results demonstrate the proposed energy-optimal braking strategy achieves prominent regeneration energy improvement than the regular constant deceleration braking strategy, and the trajectory tracking performance of the linear time-varying model predictive controller is superior to the regular PID controller. The analysis of the energy-optimal braking mechanism indicates the optimal regeneration energy operation is required to reasonably reduce the friction braking force and increasing motor braking force, while ensures the motor working at a high-efficiency point as much as possible.

In future work, we will develop a synthesis method to optimize vehicle speed and wheel braking force synchronously, i.e., integrates energy-optimal braking velocity planning problem with the braking force distribution ratio of motor and friction braking system on each wheel for improving regeneration energy further.

Acknowledgements
Not applicable.

Authors' Contributions
HD provided fundamental ideas and wrote the manuscript. WZ assisted with building up the research framework. YG was in charge of the trial and provided all support conditions. LX and YW assisted the trial and simulations. FW and YL conducted proof reading and made some critical revisions. All authors read and approved the final manuscript.

Authors' Information
Haoxuan Dong, born in 1993, is currently a PhD candidate at *School of Mechanical Engineering, Southeast University, China*. He received his M.S. degree on vehicle engineering from *Chang'an University, China*, in 2018. His research interests include connected vehicles, vehicle energy-efficient driving control, vehicle dynamics and control.

Weichao Zhuang, born in 1990, is currently an Assistant Professor at *School of Mechanical Engineering, Southeast University, China*. He received the B.S. and PhD degrees on mechanical engineering from *Nanjing University of Science and Technology, China*, in 2012 and 2017, respectively. His current research interests include vehicle dynamics and control, optimal control, clean energy vehicles, connected vehicles, and multi-agent control.

Guodong Yin, born in 1976, is currently a Professor at *School of Mechanical Engineering, Southeast University, China*. He received his PhD degree on vehicle engineering from *Southeast University, China*, in 2007. His current research interests include vehicle dynamics and control, connected vehicles, and multiagent control.

Liwei Xu, born in 1986, is currently a Research Associate at *School of Mechanical Engineering, Southeast University, China*. He received his PhD degree on mechanical engineering from *Southeast University, China*, in 2019. His current research interests include vehicle dynamics and control, autonomous vehicles, and connected vehicles.

Yan Wang, born in 1992, is currently a PhD candidate at *School of Mechanical Engineering, Southeast University, China*. He received his M.S. degree on vehicle engineering from *Nanjing University of Aeronautics and Astronautics, China*, in 2018. His current research interests include vehicle state and parameter estimation, automotive active safety control.

Fa'an Wang, born in 1990, is currently a PhD candidate at *School of Mechanical Engineering, Southeast University, China.* He received his M.S. degree on agricultural engineering from *Kunming University of Science and Technology, China*, in 2017. His current research interests include vehicle cooperative localization and control, intelligent connected vehicles.

Yanbo Lu, born in 1995, is currently a PhD candidate at *School of Mechanical Engineering, Southeast University, China*. He received his B.S. degree on mechanical engineering from *Nanjing University of Aeronautics and Astronautics, China*, in 2017. His research interests include vehicle dynamics and control, vehicle rollover prevention.

Funding
Supported by Jiangsu Provincial Key R&D Program (Grant No. BE2019004), National Natural Science Funds for Distinguished Young Scholar of China (Grant No. 52025121), National Nature Science Foundation of China (Grant Nos. 51805081, 51975118, 52002066), Jiangsu Provincial Achievement Transformation Project (Grant No. BA2018023).

Competing Interests
The authors declare no competing financial interests.

Received: 23 June 2020 Revised: 21 March 2021 Accepted: 13 August 2021
Published online: 31 August 2021

References

[1] G B Ning, X Lu, L J Zhang, et al. Method of electric powertrain matching for battery-powered electric cars. *Chinese Journal of Mechanical Engineering*, 2013, 26(3): 483-491.
[2] Z P Cano, D Banham, S Ye, et al. Batteries and fuel cells for emerging electric vehicle markets. *Nature Energy*, 2018, 3(4): 279-289.
[3] A Adepetu, S Keshav. The relative importance of price and driving range on electric vehicle adoption: Los Angeles case study. *Transportation*, 2017, 44(2): 353-373.
[4] L Ii, Y B Zhang, C Yang, et al. Model predictive control-based efficient energy recovery control strategy for regenerative braking system of hybrid electric bus. *Energy Conversion and Management*. 2016, 111: 299–314.
[5] Y M Gao Y, L P Chen, M Ehsani. Investigation of the effectiveness of regenerative braking for EV and HEV. *SAE Technical Paper* 1999, No. 1999-01-2910.
[6] J Hellgren, E Jonasson. Maximisation of brake energy regeneration in a hybrid electric parallel car. *International Journal of Electric and Hybrid Vehicles*, 2007, 1(1): 95-121.
[7] J Joy, S Ushakumari. Regenerative braking mode operation of a three-phase H-bridge inverter fed PMBLDC motor generator drive in an electric bike. *Electric Power Components and Systems*, 2018, 46(19): 2174-2188.
[8] K Kiddee, W Keyoonwong, W Khan-Ngern. An HSC/battery energy storage system-based regenerative braking system control mechanism for battery electric vehicles. *IEEJ Transactions on Electrical and Electronic Engineering*, 2019, 14(3): 457-466.
[9] J Z Zhang, C Lv, J Gou, et al. Cooperative control of regenerative braking and hydraulic braking of an electrified passenger car. *Proceedings of the*

Institution of Mechanical Engineers, Part D: Journal of Automobile Engineering, 2012, 226(10): 1289-1302.
[10] J G Guo. Development of regenerative braking for electric vehicles in China: A review. *International Journal of Electric and Hybrid Vehicles*, 2015, 7(2): 120-138.
[11] F C Sun, W Liu, H W He, et al. An integrated control strategy for the composite braking system of an electric vehicle with independently driven axles. *Vehicle System Dynamics*, 2016, 54(8): 1031-1052.
[12] W Xu, H Chen, J M Wang, et al. Velocity optimization for braking energy management of in-wheel motor electric vehicles. *IEEE Access*, 2019, 7: 66410-66422.
[13] W Li W, H Du, W Li. Driver intention based coordinate control of regenerative and plugging braking for electric vehicles with in-wheel PMSMs. *IET Intelligent Transport Systems*, 2018, 12(10): 1300-1311.
[14] Y Lian, Y Zhao, L Hu, et al. Longitudinal collision avoidance control of electric vehicles based on a new safety distance model and constrained-regenerative-braking-strength-continuity braking force distribution strategy. *IEEE Transactions on Vehicular Technology*, 2015, 65(6): 4079-4094.
[15] L H Björnsson, S Karlsson. The potential for brake energy regeneration under Swedish conditions. *Applied Energy*, 2016, 168: 75-84.
[16] G Zhao, X Peng. Variable structure control strategy research on regenerative braking for a brushless DC motor driven electric bus cruising downhill. *Journal of Advanced Manufacturing Systems*, 2014, 13(4): 223-236.
[17] G Chen, M Hua, C Zong, et.al. Comprehensive chassis control strategy of FWIC-EV based on sliding mode control. *IET Intelligent Transport Systems*, 2018, 13(4): 703-713.
[18] B Liu, L Li, X Wang, et.al. Hybrid electric vehicle downshifting strategy based on stochastic dynamic programming during regenerative braking process. *IEEE Transactions on Vehicular Technology*, 2018, 67(6): 4716-4727.
[19] A Vahidi, A Sciarretta. Energy saving potentials of connected and automated vehicles. *Transportation Research Part C: Emerging Technologies*, 2018, 95: 822-843.
[20] Y C Lin, HLT Nguyen. Adaptive neuro-fuzzy predictor-based control for cooperative adaptive cruise control system. *IEEE Transactions on Intelligent Transportation Systems*, 2020, 21(3): 1054-1063.
[21] S E Li, Q Guo, S Xu, et.al. Performance enhanced predictive control for adaptive cruise control system considering road elevation information. *IEEE Transactions on Intelligent Vehicles*, 2017, 2(3): 150-160.
[22] F Ding, H Jin. On the optimal speed profile for eco-driving on curved roads. *IEEE Transactions on Intelligent Transportation Systems*, 2018, 19(12): 4000-4010.
[23] HX Dong, WC Zhuang, BL Chen, et al. Enhanced eco-approach control of connected electric vehicles at signalized intersection with queue discharge prediction. *IEEE Transactions on Vehicular Technology*, 2021, 70(6): 5457–5469.
[24] V H Johnson. Battery performance models in ADVISOR. *Journal of Power Sources*, 2002, 110(2): 321-329.
[25] C S N Kumar, S C Subramanian. Cooperative control of regenerative braking and friction braking for a hybrid electric vehicle. *Proceedings of the Institution of Mechanical Engineers, Part D: Journal of Automobile Engineering*, 2016, 230(1): 103-116.
[26] W C Zhuang, X Zhang, D Li, et.al. Mode shift map design and integrated energy management control of a multi-mode hybrid electric vehicle. *Applied Energy*, 2017, 204: 476-488.
[27] P Falcone, F Borrelli, H E Tseng, et al. Linear time-varying model predictive control and its application to active steering systems: Stability analysis and experimental validation. *International Journal of Robust and Nonlinear Control: IFAC-Affiliated Journal*, 2008, 18(8): 862-875.
[28] F Kuhne, WF Lages, J Silva. Model predictive control of a mobile robot using linearization. *Proceedings of Mechatronics and Robotic,* 2004: 525-530.
[29] Z Chen, C C Mi, R Xiong, et.al. Energy management of a power-split plug-in hybrid electric vehicle based on genetic algorithm and quadratic programming. *Journal of Power Sources*, 2014, 248: 416-426.
[30] D Chakraborty D, A K Nandi. Finding optimal deceleration with serial regenerative braking of electric vehicle using a multi-objective genetic algorithm. *IEEE 1st International Conference on Power Electronics, Intelligent Control and Energy Systems (ICPEICES)*, IEEE, 2016: 1-6.